Evolution of sp^2 networks with substrate temperature in amorphous carbon films: Experiment and theory

R. Gago,[1,2,*] M. Vinnichenko,[1,3] H. U. Jäger,[1] A. Yu. Belov,[4,†] I. Jiménez,[5] N. Huang,[6] H. Sun,[6] and M. F. Maitz[1]
[1]*Institute of Ion Beam Physics and Materials Research, Forschungszentrum Rossendorf, PF-510119, 01314 Dresden, Germany*
[2]*Centro de Micro-Análisis de Materiales, Universidad Autónoma de Madrid, Campus de Cantoblanco, 28049 Madrid, Spain*
[3]*Physics Department, Kyiv Taras Shevchenko University, 01033 Kyiv, Ukraine*
[4]*Technische Universität Dresden, 01062 Dresden, Germany*
[5]*Instituto de Ciencia y Tecnología de Polímeros, Consejo Superior de Investigaciones Científicas, 28006 Madrid, Spain*
[6]*College of Materials Science and Engineering, Southwest Jiaotong University, 610031 Chengdu, China*
(Received 4 February 2005; revised manuscript received 13 May 2005; published 20 July 2005)

The evolution of sp^2 hybrids in amorphous carbon (a-C) films deposited at different substrate temperatures was studied experimentally and theoretically. The bonding structure of a-C films prepared by filtered cathodic vacuum arc was assessed by the combination of visible Raman spectroscopy, x-ray absorption, and spectroscopic ellipsometry, while a-C structures were generated by molecular-dynamics deposition simulations with the Brenner interatomic potential to determine theoretical sp^2 site distributions. The experimental results show a transition from tetrahedral a-C (ta-C) to sp^2-rich structures at ~500 K. The sp^2 hybrids are mainly arranged in chains or pairs whereas graphitic structures are only promoted for sp^2 fractions above 80%. The theoretical analysis confirms the preferred pairing of isolated sp^2 sites in ta-C, the coalescence of sp^2 clusters for medium sp^2 fractions, and the pronounced formation of rings for sp^2 fractions >80%. However, the dominance of sixfold rings is not reproduced theoretically, probably related to the functional form of the interatomic potential used.

DOI: 10.1103/PhysRevB.72.014120 PACS number(s): 81.05.Uw, 81.15.Jj, 68.55.−a, 71.15.Pd

I. INTRODUCTION

Hydrogen-free amorphous carbon (a-C) is a disordered mixture of carbon atoms with sp^2 and sp^3 hybridizations.[1,2] The sp^3 hybrids confer diamond-like properties (high hardness, high density, wide band gap, chemical inertness, etc.) while the sp^2 hybrids control the electronic and optical properties because the π states lie closest to the Fermi level.[3] The material with a dominance of sp^3 hybrids (>60%) is commonly referred as tetrahedral a-C (ta-C).[4]

The atomic structure of a-C is still under discussion, which is relevant in order to tune and understand the final properties of the material. In a first approximation, the structure of a-C is governed by the sp^3/sp^2 ratio but additional features like the distortion of bond distances and angles compared to ideal graphite and diamond structures, distribution of ring sizes, and arrangement of the sp^2 hybrids also have to be addressed.[5] This information is not easy to access experimentally due to the lack of medium- and long-range order in the atomic network of a-C.

Raman spectroscopy is the most common and accessible technique to study the bonding structure of a-C films.[6] However, visible Raman spectroscopy is normally used and the signal is dominated by the scattering from sp^2 sites,[7] as visible photons preferentially excite π states. In addition, the signal is controlled by the ordering of the sp^2 sites rather than by the sp^2 fraction itself,[6] which precludes a direct quantification of the sp^3 content. Although less accessible, Raman scattering from sp^3 hybrids can be enhanced by probing with UV light due to the higher photon energy.[8] Spectroscopic ellipsometry (SE) has also been proposed as a routine method to derive the sp^3 content, although it requires additional characterization to verify the validity of the model used to fit the experimental data.[9] At proper modeling, SE can yield the dielectric function of the sample, which contains the contributions from electron transitions at the energies close to Fermi level and, thus, provides information about changes in the film electronic structure.

Regarding more sophisticated techniques, a direct measurement of the sp^3/sp^2 ratio can be achieved by ^{13}C nuclear magnetic resonance (NMR),[10] but this technique requires a relatively large amount of material (~10 mg). Hence, the most extended technique to get the sp^2 content in a-C films is electron energy loss spectroscopy (EELS) near the carbon K edge,[11–16] with the additional advantage of imaging the material when performed in a transmission electron microscope.[17] NMR and EELS present the common drawback of being time-consuming and destructive methods. Another alternative method is x-ray absorption near edge spectroscopy (XANES),[18] although it presents the constraints of limited accessibility to synchrotron facilities and its surface sensitive character. XANES gives equivalent information to EELS but presents a better spectral resolution (~0.1 eV instead of ~1 eV), being able to provide additional information by resolving fine structure features in the spectra.[19] Although carbon-based films have been extensively studied by XANES[20–22] there is, up to now, no report describing in detail the XANES spectrum of ta-C.

Theoretically, the atomic structure of a-C is difficult to model due to the large variety of local bonding environments that carbon atoms can adopt. The structural properties of a-C were investigated in a series of works using, for example, Car-Parrinello *ab initio* molecular dynamics (MD)[23] or the reverse Monte Carlo technique.[24] The deposition process it-

 ©2005 The American Physical Society

self, i.e., the steady-state growth of ta-C films by hyperthermal carbon ion beams, was studied by Marks[25] and Jäger *et al.*[26] in the frame of classical MD. Such simulations of the growth process are only feasible if empirical carbon interatomic potentials are used. Marks[25] used an environment-dependent interaction potential (EDIP) for carbon, which was developed by extending the functional form previously proposed for silicon.[27] An empirical bond-order potential determined by Brenner[28] was adopted and slightly modified[29] in the MD investigations carried out by Jäger *et al.*[26] These deposition simulations provide the largest atomic ensembles described so far in the literature and are the only theoretical calculations predicting the experimental observation[30–32] of a critical growth temperature, T_c, for a sharp transition from diamond-like to graphitic-like structures. Reproducing the energy landscape of a-C, this potential, however, overestimates the density of predominantly sp^2 structures.[26]

In this work, a-C films have been grown by filtered cathodic vacuum arc (FCVA) at different substrate temperatures in order to study the resulting bonding structure in a wide range of sp^2 contents, including ta-C.[30–32] The samples were characterized by Raman, XANES, and SE. The combination of these most powerful nondestructive techniques to sample the bonding structure of a-C films is unusual and allows a detailed study of the evolution of the sp^2 networks with the growth temperature. Furthermore, the different experimental methods for computing the sp^2 content can be contrasted. In addition, the arrangement of sp^2 sites in a-C was investigated using a number of pregiven computer-generated films from Ref. 26. The comparison between the simulation and experiment addresses crucial properties of the atomic structure of a-C and is a sensitive check for the underlying theoretical approach. Growth, coalescence, and structure of sp^2 clusters versus increasing sp^2 fraction have not yet been analyzed in former deposition simulations.

II. EXPERIMENTAL METHODS

The a-C films considered in this work were prepared by FCVA at different substrate temperatures (300–700 K). Carbon ions with a mean kinetic energy of approximately 30 eV were extracted from the arc source and then accelerated towards the substrate with a pulsed bias voltage of −50 V at a frequency of 40 Hz and a pulse width of 1.5 ms. These conditions imply a nearly monoenergetic film-forming C ion beam with a mean energy of ~80 eV. The thickness of the a-C layers produced in this way ranged between 100 and 200 nm for deposition times of 40 min. A detailed description of the system can be found elsewhere.[33]

Visible micro-Raman spectra were collected with a Renishaw Ramascope 2000 spectrometer at an excitation wavelength of 514.5 nm. The laser power density on the sample was below 5 GW m^{-2} to avoid unintentional modification of the samples. The spectral resolution of this system was 1 cm^{-1} using a spectral slit width of 4 cm^{-1}.

XANES measurements were performed at the beamline SA72 of the SuperAco synchrotron at the Laboratoire pour l'Utilisation du Rayonnement Electromagnétique (LURE) in Orsay, France. The data were acquired in the total electron yield (TEY) mode by recording the sample current drained to ground and simultaneously normalized to the yield from a gold-grid located up-stream in the x-ray path. The surface normal was positioned at 55° with respect to the incoming x-ray beam. Regarding the analysis depth of XANES-TEY, it should be noted that the technique is surface sensitive but not restricted to the outermost atomic layers. The average escape depth of the electrons from insulating samples is typically 6 nm (Ref. 34) and, therefore, the TEY-XANES signal originates from the topmost ~15 nm of the sample. This represents a sampled depth around 10%–15% of the layer thickness and, therefore, should be considered representative of the bulk of the sample. Moreover, in order to disregard the influence of surface contamination, the oxygen signal was monitored in all the samples, being the O content always below 5 at. %. It is remarkable that, under appropriate storing and handling conditions, similar XANES spectra were obtained from a-C samples grown either a few days or several months before the measurements, indicating that the surface is very stable and inert in air.

The optical properties of the films were studied by SE in the photon energy range between 0.7 and 4.0 eV. The spectral behavior of the ellipsometric parameters, ψ and Δ, were acquired by a VASE spectroscopic ellipsometer (J.A. Woolam Co., Inc., USA) in the autoretarder mode.[35] The WVASE® software was used for data acquisition and processing. The fitting of the SE data was performed using a three-phase model (air/*a*-C/Si) and two different procedures were applied. The first approach assumes a Bruggeman effective medium approximation (EMA)[9] in order to quantify the sp^2/sp^3 content. The data was fitted using the optical constants of diamond[36] and pyrolithic graphite for simulation of sp^3 and sp^2 sites, respectively. The second approach gives a much better fit of the SE data and employs a parametrized semiconductor model based on the proposal by Kim *et al.*[37] In this case, a full analytical form of the electronic density of states is considered and, thus, the use of arbitrary cutoff energies is not required. The mathematical details of the parametrization method can be found elsewhere.[38] The present model goes beyond the usual approximation of Lorentzian broadening, which is known to be incorrect for elements and compounds above very low temperatures (at least, higher than 123 K),[39] and provides dielectric functions values which are consistent with Kramers-Kronig relations.

III. THEORETICAL INVESTIGATIONS

The theoretical models of a-C films used in the present investigations are results of the classical MD simulations described in Ref. 26. These simulations considered an incoming beam of hyperthermal carbon ions on a diamond substrate at different substrate temperatures. Successive impacts of up to 5000 carbon atoms at a given energy E_{ion} were simulated. The evolution of the incorporated carbon atoms in time and space was followed for a relaxation time of 15 ps after every ion impact. Periodic boundary conditions were used for the two directions perpendicular to the surface orientation. The carbon-carbon atomic interaction was described with a Brenner's analytic potential energy function

TABLE I. sp^2 cluster size distributions in the 40, 50, and 55 eV C^+ deposited films whose simulation was described in Ref. 26. The films are characterized by substrate temperature during deposition, number of deposited atoms, and their sp^3 fraction.

					sp^2 cluster size									
					1	2	3	4	5	6	7	8	9	
E_{ion}(eV)	T_s(K)	Ion impacts	Deposited atoms	sp^3 fraction[a] (%)	No. of clusters									Size (and location[b]) of larger sp^2 clusters
40	100 (run I)	1200	1176	87.3±2.2	10	58		1	1	2	1			52 (*tr*), 160 (*sr*)
	100 (run II)	1200	1175	90.3±3.6	11	53		1	2	1				199 (*sr*)
	100 (run III)	1200	1180	85.8±5.5	14	72	1	1			1			158 (*sr*)
	293 (run I)	5000	4915	56.8±11.5	32	176	5	1	3	2	1	1		28, 30,[c] 1836 (*wf*)
	293 (run II)	5000	4916	55.5±12.1	46	191	5	4	3	1[c]	2		2	14, 23, 24, 34,[c] 1541 (*wf*)
	353	3200	3147	62.3±12.7	10	127	2	3	1	1		1		273 (*itr*), 782 (*sir*)
	403	3200	3156	18.2±4.6	6	54	1	1	2					27,[c] 2157 (*wf*)
	473	5000	4886	15.5±8.9	3	49								3790 (*wf*)
	673	1200	1178	6.3±1.7	3	13	1							988 (*wf*)
	873	1200	1183	3.3±1.3	1	8								1133 (*wf*)
50	100	1200	1171	84.4±7.8	12	53	1	4		1				13 (*ir*), 252 (*sr*)
55	293 (run I)	5000	4889	63.0±15.2	54	205	19	4	3	2	1	2	2	10(2×), 14, 18, 23, 23,[c] 30,[c] 47 (*ir*), 76 (*itr*), 78 (*tr*), 458 (*sir*), 544 (*ir*)
	293 (run II)	5000	4919	55.5±15.3	50	172	17	4	3	2	2		2	13, 28, 63 (*tr*), 190 (*tr*), 234 (*sir*), 1085 (itr)

[a]The bulk value, i.e., the sp^3 fraction averaged over the inner region of the film, is given.
[b]The location is indicated only for sp^2 networks of size >45. Many SP rings exist in all these clusters. The meaning of the abbreviations used is as follows: *tr*—transition region between film and substrate, *ir*—inner film region, *sr*—film surface, *wf*—through the whole film, *itr*—from inner film region to transition region, *sir*—from surface to inner film region.
[c]These clusters contain one or two rings (with lengths ranging from 6 to 10).

(parameter set I of Ref. 28). To account for long-range effects, the Brenner potential has been modified by increasing the inner and outer C-C interaction cutoffs to $R=1.95$ Å and $S=2.25$ Å, respectively.

Dense a-C films with a large sp^3 content (60%–80%) have been normally obtained at room temperature with quasi-monoenergetic C^+ beams in the energy interval from a few tens up to some hundreds of eV, with the highest sp^3 fraction normally formed at 90–100 eV.[40,41] Under fine control of the ion energy and substrate temperature, the upper limit for ta-C growth can be even increased to the keV range.[42] The theoretical study in Ref. 26 covers and determines the critical graphitization temperature T_c for the impact energy value $E_{ion}=40$ eV, whereas in the present experiments by FCVA an average E_{ion} of ~80 eV was used, close to the optimal value for the sp^3 content. This discrepancy is not crucial for the validity of the comparative study between the experimental and theoretical results since in both cases the energy value lies within the range for ta-C growth and similar qualitative trends with substrate temperature are expected for different ion energies. This assumption is also supported by the similar theoretical results found for different ion energies by comparing the results shown in Table I for $E_{ion}=40$ and 50 eV ($T_s=100$ K) or $E_{ion}=40$ and 55 eV ($T_s=293$ K). Calculations closer to the experimental energy value were not performed due to the high CPU time requirements for deposition simulations, which are of the order of several months per film.

Columns 1–5 of Table I characterize the computer-generated a-C film samples adopted from Ref. 26. The thickness of the inner film region with steady-state properties scales with the number of deposited atoms and ranges from ~10 to ~80 Å for 1200 and 5000 atom impacts, respectively. The lateral dimensions are about 17.5×17.5 Å^2. The atom positions and neighbor lists of these samples were used to determine the sp^2 clusters (Table I) and rings (Figs. 8 and 9). An sp^2 cluster is defined as a network consisting of consecutive threefold coordinated atoms. The rings existing inside the clusters were counted using the shortest-path (SP) criterion of Franzblau.[43] "Spurious rings" arising from the use of periodic boundary conditions were identified by taking into account explicitly the atomic coordinates in addition to the neighbor lists. The shortest spurious ring which occurred consists of 14 atoms, which is just the minimum number of neighbored atoms along a zigzag line through the simulation cell.

IV. EXPERIMENTAL RESULTS

A. Visible Raman spectroscopy

Figure 1 shows the visible Raman spectra (open dots) of the a-C films considered in this work. In all cases, the spectrum consists of a broad band between 1300 and 1600 cm^{-1}. Empirically, the visible Raman spectra of a-C show two prominent features that are referred as the "*G*" (graphite) and "*D*" (disorder) peaks. The *G* peak corresponds to stretching

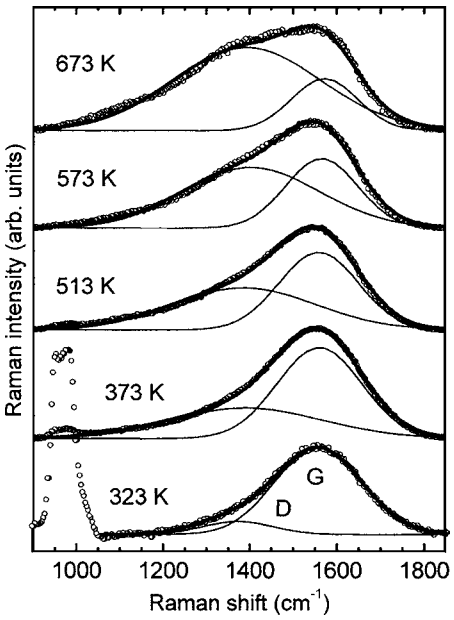

FIG. 1. Raman spectra (open dots) and the corresponding fitting curves (solid lines) for a-C films grown by FCVA at different substrate temperatures.

mode vibrations of any pair of sp^2 sites (either in -C═C- chains or in rings) while the "*D*" peak is due to a breathing mode of sixfold rings and, thus, only sp^2 sites participating in such rings contribute to this mode.[6] The *D* mode is forbidden in perfect crystalline graphite and becomes active only when disorder is present in the structure.[44] In the low temperature regime ($T<500$ K), the Raman spectrum presents a dominant *G* peak with a low intensity of the *D* peak. The sample grown at ~323 K shows a nearly zero *D* peak and a prominent second order peak at ~960 cm^{-1} from the Si substrate. This spectrum is a signature of ta-C[30] and, therefore, indicates the high sp^3 content of this sample. In the atomic structure of ta-C, where the network consists mainly of sp^3 hybrids, the small number of sp^2 sites limits the formation of clusters and, hence, the sp^2 atoms are localized on olifenic chains and, eventually, isolated sp^2 dimers within the sp^3 matrix.[45–47] This structural arrangement of sp^2 hybrids in pairs explains the reduced intensity of the peak *D* in the Raman spectra for the a-C samples grown at low temperatures (<500 K). By increasing the substrate temperature, the sp^2 hybrids arrange or cluster in aromatic rings, as indicated by the promotion of the *D* peak.

For the fitting procedure of the Raman spectra, the simplest approach of two Gaussian contributions for the *D* and *G* modes has been considered. The resulting fitting curves are shown together with the experimental data in Fig. 1 (solid lines). The choice of a Gaussian line shape instead of a Lorentzian is justified by the random distribution of phonon lifetimes in disordered materials.[6] Figure 2 shows the fitting results from Fig. 1, indicating very similar trends as those reported by Chhowalla *et al.*[30] According to the three-stage model of Ferrari *et al.*,[6] the up-shifting of the *G* peak position and the increase of the $I(D)/I(G)$ ratio indicates a transition from ta-C to a-C as the substrate temperature is increased. In addition, the order of the sp^2 hybrids is promoted with temperature as revealed by the decrease of the full width at half maximum (FWHM) of the *G* peak. In all the cases, the cluster size of the sp^2 clusters can be assumed to be below 1 nm since the FWHM exceeds 50 cm^{-1}.[1]

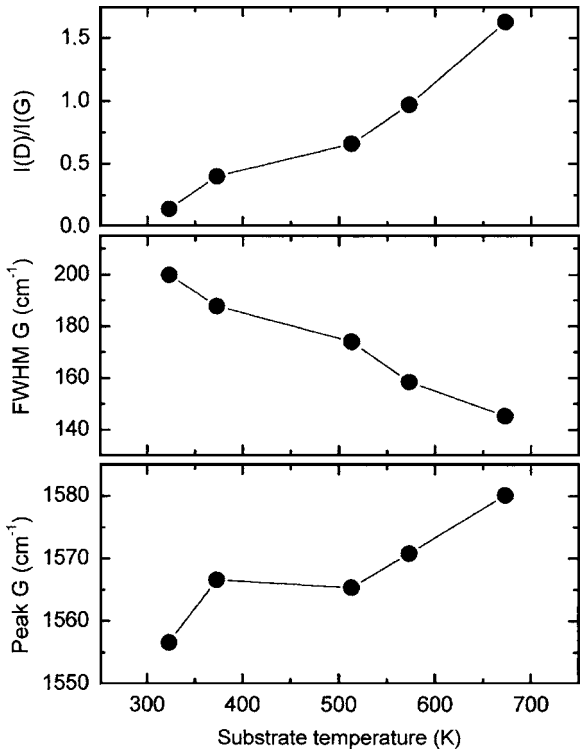

FIG. 2. Fitting results from the Raman spectra of Fig. 1.

B. X-ray absorption near edge spectroscopy

Figure 3 shows the XANES spectra of the samples considered in this work. The spectra of graphite and diamond are included as signatures of sp^2 and sp^3 hybridizations, respectively. The spectrum of graphite presents two absorption edges around 284 and 291 eV related to $1s \rightarrow \pi^*$ and $1s \rightarrow \sigma^*$ transitions, respectively. The absence of π bonding in diamond shows up as a single absorption edge with a lower energy threshold (~289 eV) than in graphite. The spectrum of an a-C film produced by electron beam evaporation (e-C) is also included as reference of a graphite-like disordered material. In all the a-C samples, there is a weak peak at 286–288 eV related to a small contribution of surface contamination from CO_x moieties.[48] The onset of the σ^* edge at ~288 eV and the reduced intensity in the π^* region for the sample grown at room temperature (323 K) indicate a dominant sp^3 character. Therefore, in agreement with the Raman results, this sample can be cataloged as ta-C.

A deeper insight in the evolution of the bonding structure can be derived from the fine structure in the π^* region of the XANES spectra, as shown in Fig. 4. The promotion of sp^2 hybrids with substrate temperature is evidenced by the overall increase of the intensity of π^* states. Parallel, the same trend is derived from the appreciable shift of the threshold energy at the σ^* edge to higher values in Fig. 3. In the magnified π^* region, a weak shoulder is observed for the samples

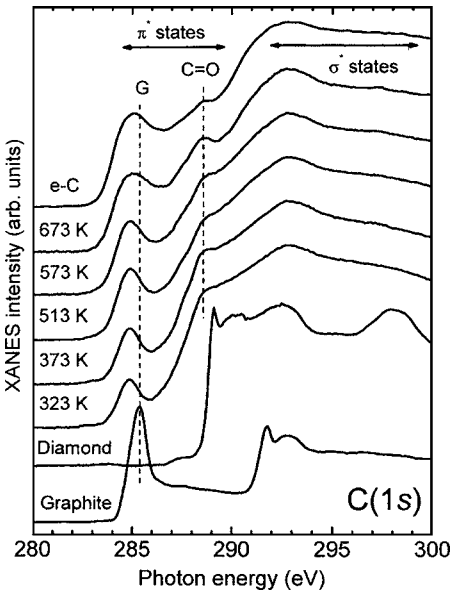

FIG. 3. XANES spectra of a-C films deposited by FCVA at different substrate temperatures together with the reference spectra of diamond and graphite. A sample grown by electron-beam evaporation of graphite (e-C) is also shown as representation of a ~100% sp^2 disordered material.

with the higher sp^3 content below the π^* resonance (feature *A* in Fig. 4). The presence of this feature has also been observed by EELS and, although its nature is still unclear, it has been attributed to dangling bonds or core-level excitons.[12,14] The π^* resonance for the ta-C sample (323 K) is at 284.9 eV (peak *B*), below the position corresponding to graphitic environments at 285.4 eV (feature *G*). This downshifting of the resonance position was also reported previously by EELS,[12] although a clear assignment of this trend has not been given. A plausible explanation could be the presence of sp^2 chains or isolated sp^2 pairs (based on the atomic structure of sp^3 rich networks), and/or defects in the graphitic network such as vacancies or bond angle distortions. However, it should be noted that the position of the π^* resonance for disordered

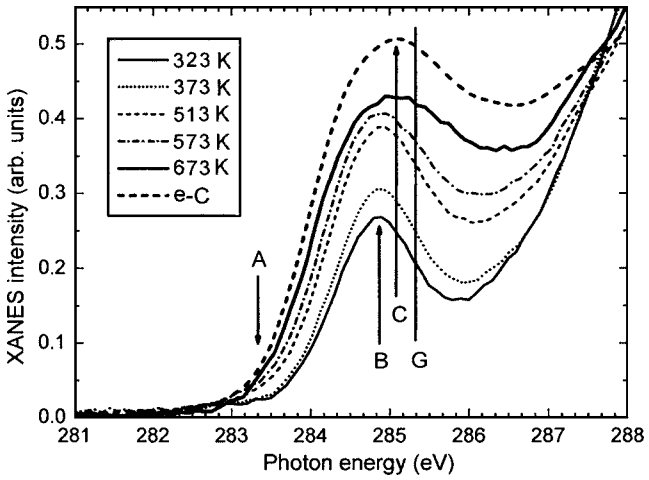

FIG. 4. Detailed view of the π^* region of the XANES spectra displayed in Fig. 3.

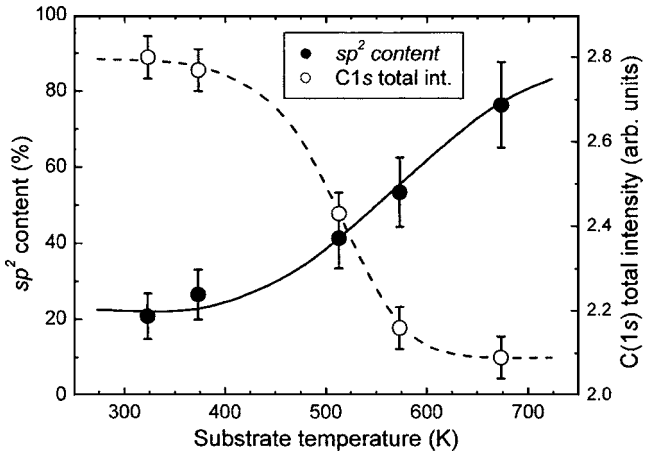

FIG. 5. Calculated sp^2 content from the XANES spectra (●) and total intensity of the C(1*s*) edge (○). The lines are a guide to the eye to evidence the transition from diamond-like to graphite-like structures starting at ~500 K.

graphitic environments, as evidenced by the e-C sample (peak *C*), appears also below that of graphite (~285.2 eV) but with an energy shift of ~0.3 eV with respect to the main feature at ~284.9 eV. This trend reinforces the assignment of peak *B* to sp^2 chains or pairs. Moreover, peak *B* dominates in the π^* region up to temperatures of ~600 K, since only in the sample grown at 673 K the intensity at ~285.2 eV (feature *C*) increases appreciably. This means that the sp^2 arrangement is dominated by isolated pairs or small olefinic clusters (chain-like arrangements) for substrate temperatures below 600 K. Above 600 K, the promotion of feature *C* corresponds to the promotion of disordered graphite-like environments and, hence, reveals the formation of rings.

In analogy with EELS, the sp^2 content computed by XANES considers the relative intensity of the π^* and σ^* states regions. This method assumes that the intensity of the π^* states is proportional to the number of π-bonded electrons in the material and, hence, to the number of sp^2 sites.[24] Assuming the same sensitivity factor for π^* and σ^* states, the π^*/σ^* intensity for 100% sp^2 and sp^3 materials should be 1/3 and 0/4, respectively. However, in practice, there is no appropriate theory to predict the π^*/σ^* ratio and a reference material with known sp^2 content is required for quantitative analysis. Graphite cannot be used due to the excitonic character of the π^* resonance and the dependence of its intensity on the orientation of the basal planes with respect to the incoming x-ray beam.[18] For this reason, some authors have also considered for quantification the use of fullerene films[16] or a disordered form of graphite.[49] As a reference material, we have preferred to use the spectrum of e-C since it has a disordered structure similar to the samples presented here. This sample is assumed to have an sp^2 content of 95±5%.[10]

In order to get an accurate calculation of the relative π^*/σ^* XANES intensity from the spectra of Fig. 3 several considerations should be taken into account. First, there is some overlap of the π^* and σ^* signals that tends to overestimate the sp^2 content and that is more significant when the π^* intensity is smaller (higher sp^3 content). In order to reduce this effect, special attention has been paid to the inte-

gration limits and the σ^* edge was subtracted before integration of the π^* region. Particularly, the 282–286 eV and 289–295 eV regions has been considered for the π^* and σ^* intensities, respectively. Second, there might be distortion in the TEY-XANES spectral shape as compared with the true absorption signal that would be obtained in transmission measurements. This deviation occurs when the electron emission is not directly proportional to the photoabsorption and, among other factors, it may be the result of saturation in the TEY signal due to self-absorption effects.[50] The self-absorption effect originates from the unequal penetration depth (λ_x) with the photon energy and saturation in TEY is significant when the electron escape depth (λ_e) is similar or larger than λ_x. The removal of this effect is difficult and implies the exact knowledge of λ_e and λ_x to introduce in the spectral line shape an energy-dependent correction factor. This procedure requires a reference spectrum of the material under study measured in transmission mode, which is not available in this case. Qualitatively, saturation would affect mainly the σ^* edge (minimum λ_x), as already observed in graphite by comparison of TEY with fluorescence and transmission measurements.[51] This effect should have a larger contribution in predominantly sp^3 samples, due to a higher density and their insulating character (higher electron depth escape[52]). From computed λ_x values,[53] the saturation effect could account in the worst case for an underestimation of the σ^* intensity by ~10% and ~5% in sp^3-rich samples and sp^2-rich samples, respectively. However, in practice, the error introduced in the sp^2 content due to saturation effects should be lower since the same systematic error is affecting the reference sample (e-C) considered for the quantification of the sp^2 content.

The solid dots in Fig. 5 show the evolution with temperature of the sp^2 content, as computed from the XANES spectra. The data show a clear structural transition from diamond-like (ta-C) to graphitic-like carbon with a transition threshold at $T_c \sim 500$ K. A complete graphitization of the structure ($sp^2 > 80\%$) is obtained for temperatures above 600 K. The value of T_c may be dependent on the ion energy and the deposition rate.[2] A value of ~423 K was measured for the growth of ta-C films with an ion energy of 120 eV by Lifshitz *et al.*,[31] whereas Chhowalla *et al.*[30] reported a T_c of ~500 K for an ion energy of 90 eV. Therefore, our results with ~80 eV are in line with those of other groups.

The total photoelectron yield measured during XANES measurements in sp^2/sp^3 mixtures increases with the fraction of sp^3 hybrids[54] and, therefore, it provides further metric of the sp^2 content. This effect is related with a lower average work function of the surface in sp^2/sp^3 mixtures with the promotion of sp^3 hybrids.[54] As displayed in Fig. 5 (open dots), the value of the TEY signal recorded during our XANES experiments follows the opposite trend of the computed sp^2 content, in agreement with the previous assumptions and corroborating the transition threshold at ~500 K. In the case of pure segregated sp^2 and sp^3 carbon phases, the enhancement of the TEY signal is found to be ~8 times for the sp^3 phase (diamond) with respect to the sp^2 phase (graphite).[54] In our case, the increase in the signal for diamond-like films is only ~40% higher than for graphite-like structures. This is an indication of the atomic mixture of sp^2 and sp^3 hybrids and, therefore, that phase segregation is not significant here.

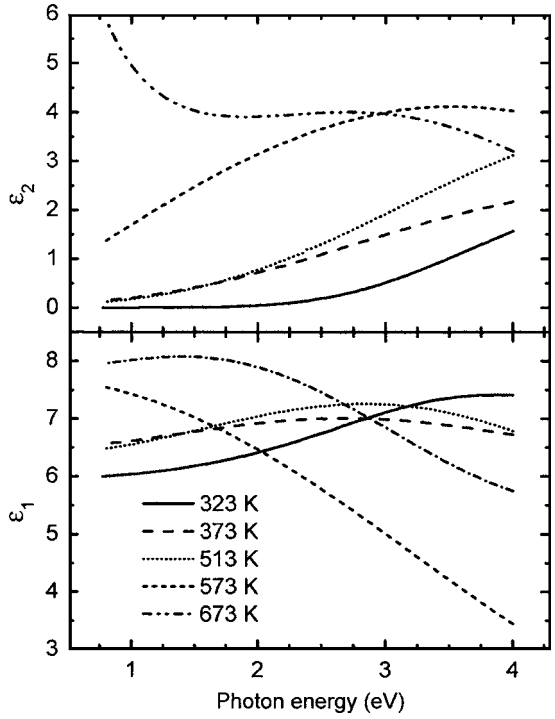

FIG. 6. Complex dielectric function derived from SE measurements.

C. Spectroscopic ellipsometry

The dielectric function of a-C films is directly related to $\pi \rightarrow \pi^*$ and $\sigma \rightarrow \sigma^*$ transitions in the visible and ultraviolet energy ranges, respectively,[55] and can be directly extracted from SE measurements. Figure 6 shows the complex dielectric function derived from SE for the samples considered in this work. The real, ε_1, and imaginary, ε_2, values are in good agreement with the data reported by other authors for ta-C films.[56]

Most of the information can be extracted from ε_2, since it gives a measure of the optical transition strength, $\omega^2 \varepsilon_2(\omega)$, where ω is the probing light frequency. This value is related through the integral transformation to the density of states of the valence and conduction bands.[56] The ε_2 spectrum for the sample grown at 323 K presents no absorption below 3 eV and indicates a wide band-gap material, as expected from its diamond-like structure. The presence of the absorption band around 3.8 eV in the ε_2 spectra is related to $\pi \rightarrow \pi^*$ electronic transitions and it is a signature of sp^2 sites.[55] However, this energy position is different from the energy of $\pi \rightarrow \pi^*$ transitions in crystalline graphite which occur at 4.5 eV.[57,58] This shift is attributed to the loss of the *k*-selection rule in the amorphous state[55] or to a different arrangement of the sp^2 sites.[59] The former argument is in agreement with the observation by Raman and XANES of the sp^2 hybrids to form preferentially chain-like structures rather than rings. The intensity around 3.8 eV increases with the substrate temperature in correlation with the promotion of sp^2 hybrids observed by Raman and XANES, but also in line with the

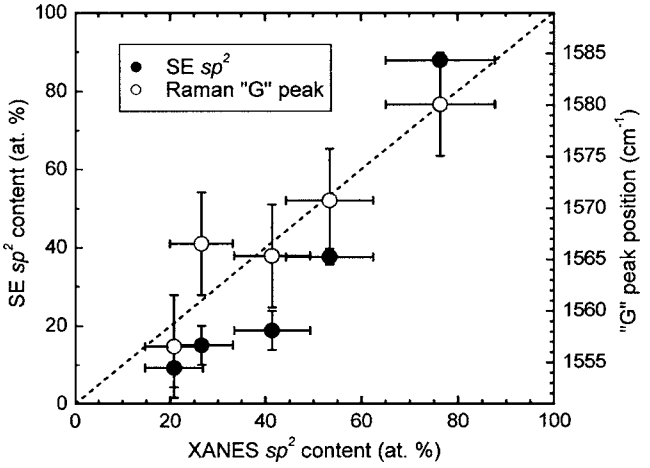

FIG. 7. Comparison of the SE (●) and Raman (○) results with the sp^2 content calculated by XANES.

clustering and formation of sixfold rings. The increase is most pronounced for the sample grown above T_c, as expected from the graphitization process.

The dielectric function of the sample produced at 673 K has a graphite-like spectral behavior.[57] In this case, the SE data fitting requires the inclusion of a Drude-term to provide good agreement between the measured and simulated values in the near-infrared region. Therefore, the strong increase in ε_2, as well as in the optical transition strength below 1 eV for the sample deposited at 673 K, indicates the enhancement of the contribution from free electrons absorption to the pseudo-dielectric function and points to a higher conductivity of this sample. This trend should be related with the formation of extended graphite-like domains (planar sp^2 clusters) and should be correlated with the promotion of feature *C* in the XANES spectra of Fig. 4.

V. DISCUSSION

A. Evolution of measured sp^2 arrangements

The combination of the different experimental techniques used in this work allows us to follow the evolution of the sp^2 arrangements with substrate temperature and check the accuracy and limitations of the different methods used. Figure 7 compares the sp^2 content obtained by XANES with the results from SE and Raman spectroscopy and shows a good correlation between the indicators used in the different techniques. As already mentioned, the EMA approach provides much worse fit than the parametric semiconductor model for the evaluation of the SE data and, therefore, the sp^2 content should be considered only as an estimate. Due to the use of diamond and graphite optical constants to simulate sp^3 and sp^2 sites, respectively, the sp^2 content is underestimated for low sp^2 contents ($<50\%$) and overestimated for high ($>50\%$) sp^2 contents. Despite this fact, the values are in relatively good agreement with the XANES data. In the case of Raman spectroscopy, the variation of the *G* peak (see Fig. 2) can be related with the bond length and, corroborating the above assumptions, increases following the trend in the sp^2 content (see Fig. 7).[6]

It can be concluded that the bonding structure evolves from a diamond-like structure to a graphitic-like structure at temperatures above a threshold of ~500 K. However, it has been shown that the arrangement of the sp^2 hybrids is dominated by isolated pairs or small olefinic (chain-like) structures up to temperatures below 600 K, thus, even when the structure is not diamond-like anymore (sp^2 content $>50\%$). These findings contrast with the cluster-model proposed to explain the atomic structure of a-C, where ring arrangements should be preferred to linear clusters.[5] However, similar conclusions to those presented here follow from the theoretical calculations of Frauenheim *et al.*[60]

It is interesting to note that the arrangement of sp^2 hybrids is not directly correlated with the sp^2 content, as previously observed by Ferrari *et al.*[6] In our case, we observe that olefinic environments prevail, as shown by the position of the π^* resonance in the XANES spectra at ~284.9 eV (feature *B* in Fig. 4) and the lack of π conjugation shown by SE (Fig. 6). This contrasts with the detection of sp^2 rings by Raman spectroscopy (promotion of peak *D*) at temperatures lower than 600 K, which should be attributed to the high sensitivity of Raman spectroscopy to this arrangement and that the evolution of medium-range order (development of graphitic domains) only takes place for temperatures above 600 K.

B. Network calculations by MD simulations

The combination of Raman, XANES, and SE investigations in the present work provides a rather precise value for the threshold temperature. The resultant temperature of $T_{c,\mathrm{exp}} \sim 500$ K for the growth at ~80 eV exceeds significantly the theoretical result of $T_{c,th} \sim 373$ K at $E_{ion}=40$ eV, which follows from the MD deposition simulations if column 5 of Table I is considered. This discrepancy, already mentioned in Ref. 26 where it was still less evident, is not surprising. A temperature difference of ~130 K corresponds to a kinetic energy difference of only ~13 meV per atom. The consideration of the effect of such small energy differences on the deposition process is at the accuracy limit of the present MD model. Figure 9 of Ref. 26 reveals that the statistical fluctuations in the computed average potential energies of bulk atoms in different films are of the same order of magnitude. To overcome this problem in the subsequent discussion, the computed temperature values will no longer be used as reference parameters. Instead, the network properties will be discussed versus the sp^3 fraction (column 5 of Table I).

The last columns of Table I present the size distributions of all sp^2 clusters occurring in the theoretical films. Let us first comment on the samples with sp^3 fractions exceeding 80% in the inner film region. In such structures, large sp^2 networks (with more than seven atoms) are predicted to exist only in the sp^2-rich surface region[26] or in the transition region to the substrate. In the bulk, most of the sp^2 sites ($>75\%$) form pairs. In addition, there are a few single threefold coordinated atoms corresponding to sp^3 hybrids with dangling bonds and a very few other clusters of size 3–7. This sp^2 cluster size distribution is in good qualitative agreement with the experimental results presented here. An iso-

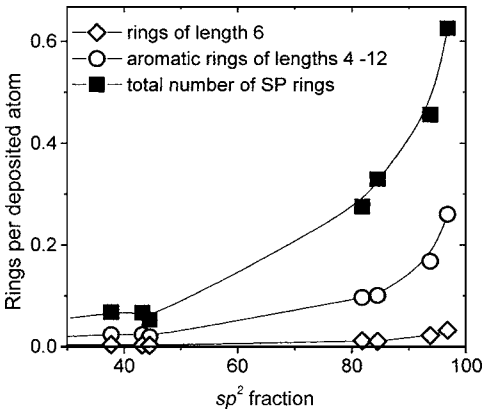

FIG. 8. SP ring frequencies from MD simulated films as a function of the sp^2 fraction. The deposition energy of all these films was 40 eV. The lines are plotted as "guide to the eye."

lated pair of sp^2 hybrids does not constitute a strong distortion in ta-C and it is realized by the formation of one nonconjugated C-C double bond within a network of sp^3 hybridized atoms.

As the sp^3 fraction reduces to $\sim$60%, the sp^2 hybrids coalesce, indicated by the considerable increase in the sizes and frequencies of larger sp^2 clusters (Table I). Such a process was identified by Huang *et al.*[61] who performed ultraviolet and visible Raman spectroscopy investigations of diamond-like carbon films grown by pulsed laser deposition. They stated that the sp^2 sites begin to condense into clusters of increasing size with the sp^3-bonded carbon atoms still being predominant. In our samples, an sp^2 network extended over the whole film begins to arise for sp^3 contents of $\sim$55% (abbreviation "*wf*" in the last column of Table I).

The extended sp^2 networks crossing the films or even dominating them (see the samples in Table I with sp^3 fractions $<$20%) contain many rings. Figures 8 and 9 show the total number of SP rings and size distributions of the rings as a function of the sp^2 fraction, respectively. Considering the ring frequencies plotted in Fig. 8, the simulations predict a pronounced increase of ring numbers for sp^2 fractions $>$80% in accordance with the experimental results. However, in contrast with the experimental data, the broad theoretical ring size distributions given in Fig. 9 are not peaked at six-fold rings but, instead, at larger rings of lengths 8–12. This model result is inconsistent with the proper asymptotic behavior of ring sizes in the direction to graphite-like structures with an sp^2 content approaching 100%. The incorrect theoretical peak position found here[62] is probably related to the functional form of the interatomic potential used. The potential of Brenner incorporates conjugation in an approximate way, with the distinction between conjugated and nonconjugated double bonds being controlled by the parameter N_{ij}^{conj}. The subtle differences in bond orders for conjugated ring systems, however, remained beyond the accuracy of this approximation.[28] According to Glosli and Ree,[63] adding a torsional energy term for rotations about π bonds to the Brenner potential, one can tailor the relative stability of sp^2 liquid or amorphous carbon phases. This term, absent in the original version of the Brenner potential (and in the deposition simulations of Ref. 26), would force the sp^2 structures to be planar. Marks published ring statistics for various densities (2.6–3.2 g cm^{-3}) of a-C networks generated not by beam deposition but by liquid quenching using his more recent empirical potential (EDIP),[25] which also accounts for the torsion effects neglecting, however, conjugation. These ring distributions (see Fig. 12 in Ref. 25) are correctly peaked at a ring length of 6, indicating that the torsion effects appear to be more important for the correct prediction of ring statistics than conjugation.

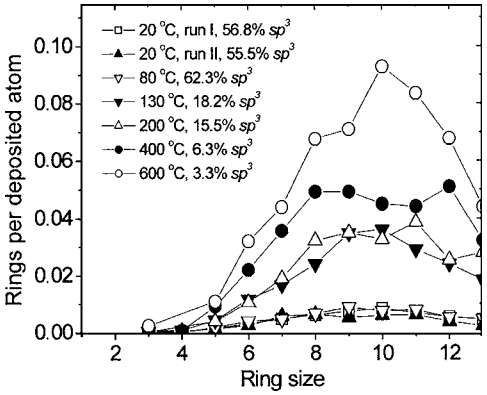

FIG. 9. Size distributions of SP rings of sp^2 atoms in the MD simulated films which contain one spacious sp^2 network throughout the whole film.

VI. CONCLUSIONS

The bonding structure of a-C films prepared by FCVA at different substrate temperatures has been studied by Raman spectroscopy, XANES and SE. This combination allows a detailed study of the evolution of the sp^2 arrangements with substrate temperature. The experimental results show a transition from diamond-like to graphitic-like structures with a temperature threshold of $\sim$500 K. The sp^2 arrangements are dominated by pair and/or small olefinic-like structures (chain-like) up to $\sim$600 K, even when the sp^2 fraction increases up to 50%. The arrangement in graphite-like environments is only evident for temperatures above 600 K and, therefore, sp^2 contents exceeding 80%. This trend might be explained by the evolution of the medium-range order with substrate temperature and the rearrangement of the local-order bonding for temperatures above 600 K. The theoretical analysis of sp^2 clusters and rings in samples generated by MD deposition simulations reproduces these results to a large extent. The transition from isolated sp^2 pairs to a continuous and dominant sp^2 network is quantitatively shown. However, the theoretical results do not reproduce the asymptotic behavior of ring sizes in the direction to graphite-like structures for large sp^2 contents ($>$80%).

ACKNOWLEDGMENTS

We are indebted to P. Parent and C. Laffon for their help with the XANES measurements at LURE. The synchrotron work was financed by the EU-TMR program. This work was also partially financed by YS INTAS (Grant No. 01/2-113) and the National Natural Science Foundation of China (Grant No. NSFC30270392).

*Corresponding author. E-mail: raul.gago@uam.es (TF/FAX: +34 91 497 3621/3623)
†Permanent address: Institute of Crystallography RAS, Moscow, Russia.

[1] J. Robertson, Mater. Sci. Eng., R. **37**, 129 (2002).
[2] Y. Lifshitz, Diamond Relat. Mater. **8**, 1659 (1999).
[3] J. Robertson, Phys. Rev. Lett. **68**, 220 (1992).
[4] D. R. McKenzie, Rep. Prog. Phys. **59**, 1611 (1996).
[5] J. Robertson and E. P. O'Reilly, Phys. Rev. B **35**, 2946 (1987).
[6] A. C. Ferrari and J. Robertson, Phys. Rev. B **61**, 14095 (2000).
[7] N. Wada, P. J. Gaczi, and A. Solin, J. Non-Cryst. Solids **35/36**, 543 (1980).
[8] K. W. Gilkes, H. S. Sands, D. N. Batchelder, J. Robertson, and W. I. Milne, Appl. Phys. Lett. **70**, 1980 (1997).
[9] J. Lee, R. W. Collins, V. S. Veerasamy, and J. Robertson, Diamond Relat. Mater. **7**, 999 (1998).
[10] H. Pan, M. Pruski, B. C. Gerstein, F. Li, and J. S. Lannin, Phys. Rev. B **44**, 6741 (1991).
[11] J. J. Cuomo, J. P. Doyle, J. Bruley, and J. C. Liu, Appl. Phys. Lett. **58**, 466 (1991).
[12] P. J. Fallon, V. S. Veerasamy, C. A. Davis, J. Robertson, G. A. J. Amaratunga, W. I. Milne, and J. Koskinen, Phys. Rev. B **48**, 4777 (1993); **49**, 2287(E) (1993).
[13] J. Kulik, Y. Lifshitz, G. D. Lempert, J. W. Rabalais, and D. Marton, J. Appl. Phys. **76**, 5063 (1994).
[14] J. Kulik, G. D. Lempert, E. Grossman, D. Marton, J. W. Rabalais, and Y. Lifshitz, Phys. Rev. B **52**, 15812 (1995).
[15] A. C. Ferrari, A. Libassi, B. K. Tanner, V. Stolojan, J. Yuan, L. M. Brown, S. E. Rodil, B. Kleinsorge, and J. Robertson, Phys. Rev. B **62**, 11089 (2000).
[16] A. J. Papworth, C. J. Kiely, A. P. Burden, S. R. P. Silva, and G. A. J. Amaratunga, Phys. Rev. B **62**, 12628 (2000).
[17] R. F. Egerton, *Electron Energy Loss Spectroscopy in the Electron Microscope* (Plenum, New York, 1986).
[18] J. Stöhr, *NEXAFS Spectroscopy* (Springer, Berlin, 1992).
[19] I. Jiménez, R. Gago, and J. M. Albella, Diamond Relat. Mater. **12**, 110 (2003).
[20] F. L. Coffman, R. Cao, P. A. Pianetta, S. Kapoor, M. Kelly, and L. J. Terminello, Appl. Phys. Lett. **69**, 568 (1996).
[21] R. Gago, I. Jiménez, and J. M. Albella, Surf. Sci. **482-485**, 530 (2001).
[22] I. Jiménez, R. Gago, J. M. Albella, and L. J. Terminello, Diamond Relat. Mater. **10**, 1170 (2001).
[23] D. G. McCulloch, D. R. McKenzie, and C. M. Goringe, Phys. Rev. B **61**, 2349 (2000).
[24] J. K. Walters, K. W. R. Gilkes, J. D. Wicks, and R. J. Newport, Phys. Rev. B **58**, 8267 (1998).
[25] N. Marks, J. Phys.: Condens. Matter **14**, 2901 (2002).
[26] H. U. Jäger and A. Yu. Belov, Phys. Rev. B **68**, 024201(2003).
[27] N. A. Marks, Phys. Rev. B **63**, 035401 (2000).
[28] D. W. Brenner, Phys. Rev. B **42**, 9458 (1990); **46**, 1948 (1992).
[29] H. U. Jäger and K. Albe, J. Appl. Phys. **88**, 1129 (2000).
[30] M. Chhowalla, A. C. Ferrari, J. Robertson, and G. A. J. Amaratunga, Appl. Phys. Lett. **76**, 1419 (2000).
[31] Y. Lifshitz, G. D. Lempert, S. Rotter, I. Avigal, C. Uzan-Saguy, and R. Kalish, Diamond Relat. Mater. **2**, 285 (1993).
[32] S. Sattel, J. Robertson, and H. Ehrhardt, J. Appl. Phys. **82**, 4566 (1997).
[33] Y. X. Leng, J. Y. Chen, P. Yang, H. Sun, G. J. Wan, and N. Huang, Surf. Coat. Technol. **173**, 67 (2003).
[34] D. G. J. Sutherland, H. Akatsu, M. Copel, F. J. Himpsel, T. A. Callcot, J. A. Carlisle, D. L. Ederer, J. J. Jia, I. Jiménez. R. C. C. Perera, D. K. Shuh, L. J. Terminello, and W. M. Tong, J. Appl. Phys. **78**, 6761 (1995).
[35] B. Johs, J. A. Woollam, C. M. Herzinger, J. Hilfilker, R. Synowicki, and C. L. Bungay, Crit. Rev. Opt. Sci. Technol. **CR72**, 29 (1999).
[36] *Handbook of Optical Constants of Solids*, edited by E. D. Palik (Academic Press, Boston, 1996).
[37] C. C. Kim, J. W. Garland, H. Abad, and P. M. Raccah, Phys. Rev. B **45**, 11749 (1992).
[38] C. M. Herzinger and B. D. Johs, U.S.-Patent 5796983, 1998.
[39] J. W. Garland, H. Abad, M. Viccaro, and P. M. Raccah, Appl. Phys. Lett. **52**, 1176 (1988).
[40] R. Lossy, D. L. Pappas, R. A. Roy, J. P. Doyle, J. J. Cuomo, and J. Bruely, J. Appl. Phys. **77**, 4750 (1995).
[41] S. R. P. Silva, S. Xu, B. X. Tay, H. S. Tan, and W. I. Milne, Appl. Phys. Lett. **69**, 491 (1996).
[42] E. Grossman, G. D. Lempert, J. Kulik, D. Marton, J. W. Rabalais, and Y. Lifshitz, Appl. Phys. Lett. **68**, 1214 (1996).
[43] D. S. Franzblau, Phys. Rev. B **44**, 4925 (1991).
[44] F. Tuinstra and J. K. Koening, J. Chem. Phys. **53**, 1126 (1970).
[45] N. A. Marks, D. R. McKenzie, B. A. Pailthorpe, M. Bernasconi, and M. Parrinello, Phys. Rev. B **54**, 9703 (1996).
[46] K. W. R. Gilkes, P. H. Gaskell, and J. Robertson, Phys. Rev. B **51**, 12303 (1995).
[47] D. A. Drabold, P. A. Fedders, and P. Stumm, Phys. Rev. B **49**, 16415 (1994).
[48] I. Jiménez, D. G. J. Sutherland, A. van Buuren, J. A. Carlisle, L. J. Terminello, and F. J. Himpsel, Phys. Rev. B **57**, 13167 (1998).
[49] R. Gago, I. Jiménez, J. M. Albella, A. Climent-Font, D. Cáceres, I. Vergara, J. C. Banks, B. L. Doyle, and L. J. Terminello, J. Appl. Phys. **87**, 8174 (2000).
[50] R. Nakajima, J. Stöhr, and Y. U. Idzerda, Phys. Rev. B **59**, 6421 (1999).
[51] D. A. Fischer, R. M. Wentzcovitch, R. G. Carr, A. Continenza, and A. J. Freeman, Phys. Rev. B **44**, 1427 (1991).
[52] W. Gudat and C. Kunz, Phys. Rev. Lett. **29**, 169 (1972).
[53] Calculated using computed values from Center for x-ray Optics, Lawrence Berkeley National Laboratory, http://www.cxro.lbl.gov.
[54] I. Jiménez, R. Gago, M. M. García, and J. M. Albella, J. Vac. Sci. Technol. B **19**, 1358 (2001).
[55] S. Logothetidis, Diamond Relat. Mater. **12**, 141 (2003).
[56] F. Xiong, Y. Y. Wang, and R. P. H. Chang, Phys. Rev. B **48**, 8016 (1993).
[57] A. B. Djurisic and E. H. Li, J. Appl. Phys. **85**, 7404 (1999).
[58] S. Logothetidis, J. Petalas, and S. Ves, J. Appl. Phys. **79**, 1040 (1996).
[59] M. Gioti, D. Papadimitriou, and S. Logothetidis, Diamond Relat. Mater. **9**, 741 (2000).
[60] T. Frauenheim, P. Blaudeck, U. Stephan, and G. Jungnickel, Phys. Rev. B **48**, 4823 (1993).
[61] S. M. Huang, Z. Sun, Y. E. Lu, and M. H. Hong, Appl. Phys. A: Mater. Sci. Process. **74**, 519 (2002).
[62] sp^2 ring size distributions from ta-C deposition simulations, as presented in Fig. 9 of this paper, have not been published in the literature up to now.
[63] J. N. Glosli and F. H. Ree, Phys. Rev. Lett. **82**, 4659 (1999).